A Unified Model for Fibers With Divergent Pullout Behaviors in Strain Hardening Cementitious Composites (SHCC)

Peiyun She, Jiajie Wang, Zhiming Pang and Cong Lu *

*School of Civil Engineering, Southeast University, Nanjing, China*

Strain Hardening Cementitious Composites (SHCC) are materials exhibiting high tensile ductility with the formation of multiple cracks. Since the mechanical properties of SHCC members are governed by the interfacial characteristics between fibers and matrix, understanding the mechanism of single fiber pullout behavior is crucial for SHCC material design. Existing model was set up based on Polyvinyl Alcohol (PVA) fibers, making it inapplicable to other kinds of synthetic fibers those exhibit divergent pullout behaviors. As a result, the simulated curves cannot agree well with the tested results of SHCC made with other fibers or hybrid fibers. In this study, a unified single fiber pullout model was proposed to take divergent kinds of fiber pullout behavior into account. Five parameters were defined to describe the single fiber pullout behavior, where the frictional strength during the pullout stage and the blocking length of fiber under pulley force were for the first time introduced. For verification purpose, fiber-pullout samples with Polyethylene terephthalate (PET) and PVA fibers were tested and the results agree well with the simulated curves from proposed model. The stochasticity of each parameters were then analyzed and described by normal distribution, through which fibers with various random pullout behaviors can be incorporated into a larger scale modelling. Therefore, the fiber-bridging constitutive law for a single crack was calculated and compared with the single crack test results, which confirmed again the validity of the proposed model.

Keywords: physical model, SHCC, fiber pullout, PET fiber, PVA fiber

INTRODUCTION

Due to the quasi-brittle nature, traditional cementitious materials are vulnerable to cracking (Li et al., 2003; Jun et al., 2006; Zhigang, 2020a). Hence, fibers are added to control the cracks and improve toughness (Graybeal, 2006). With moderate fiber content added, Strain Hardening Cementitious Composites (SHCC) was developed in the 1990s (Li and Leung, 1992; Li and Wu, 1992; Victor and Forii, 1993; Leung, 1996; Li et al., 2001; Li, 2011; Victor and Li, 2012; Zhigang, 2021), which exhibits strain hardening behavior accompanied by the formation of multiple cracks and ensures the high ductility and durability of the structure.

In order to explain the strain hardening behavior in SHCC, the design criterion for SHCC including fiber, matrix and interface parameters have been proposed by Li first (Victor and Li, 2012). The most fundamental property of SHCC is the fiber bridging constitutive law which can be derived from modeling a single fiber pullout behavior against the surrounding matrix. Since the initial fiber
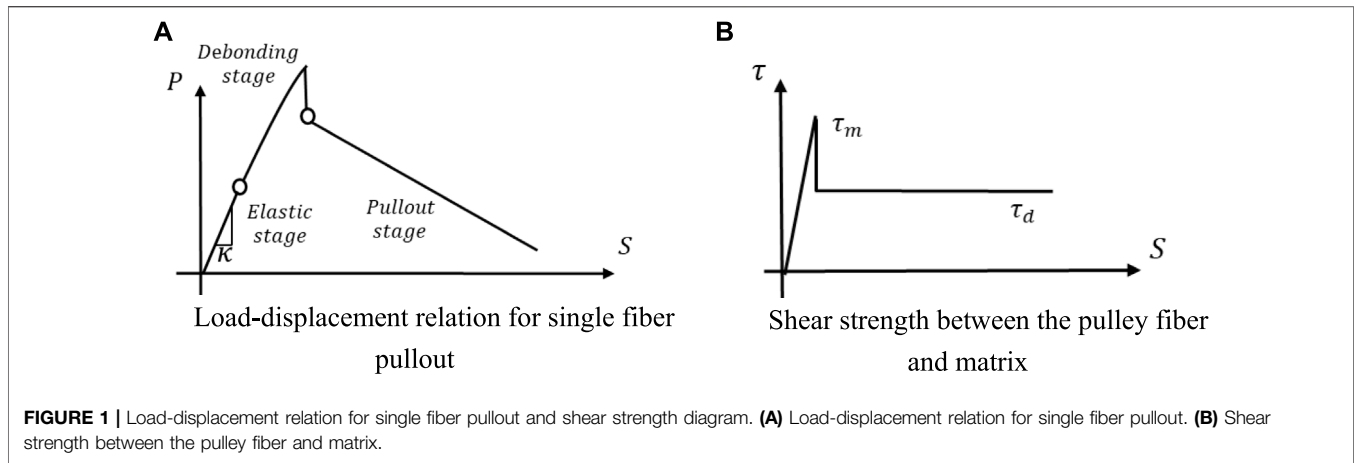
FIGURE 1 | Load-displacement relation for single fiber pullout and shear strength diagram. **(A)** Load-displacement relation for single fiber pullout. **(B)** Shear strength between the pulley fiber and matrix.
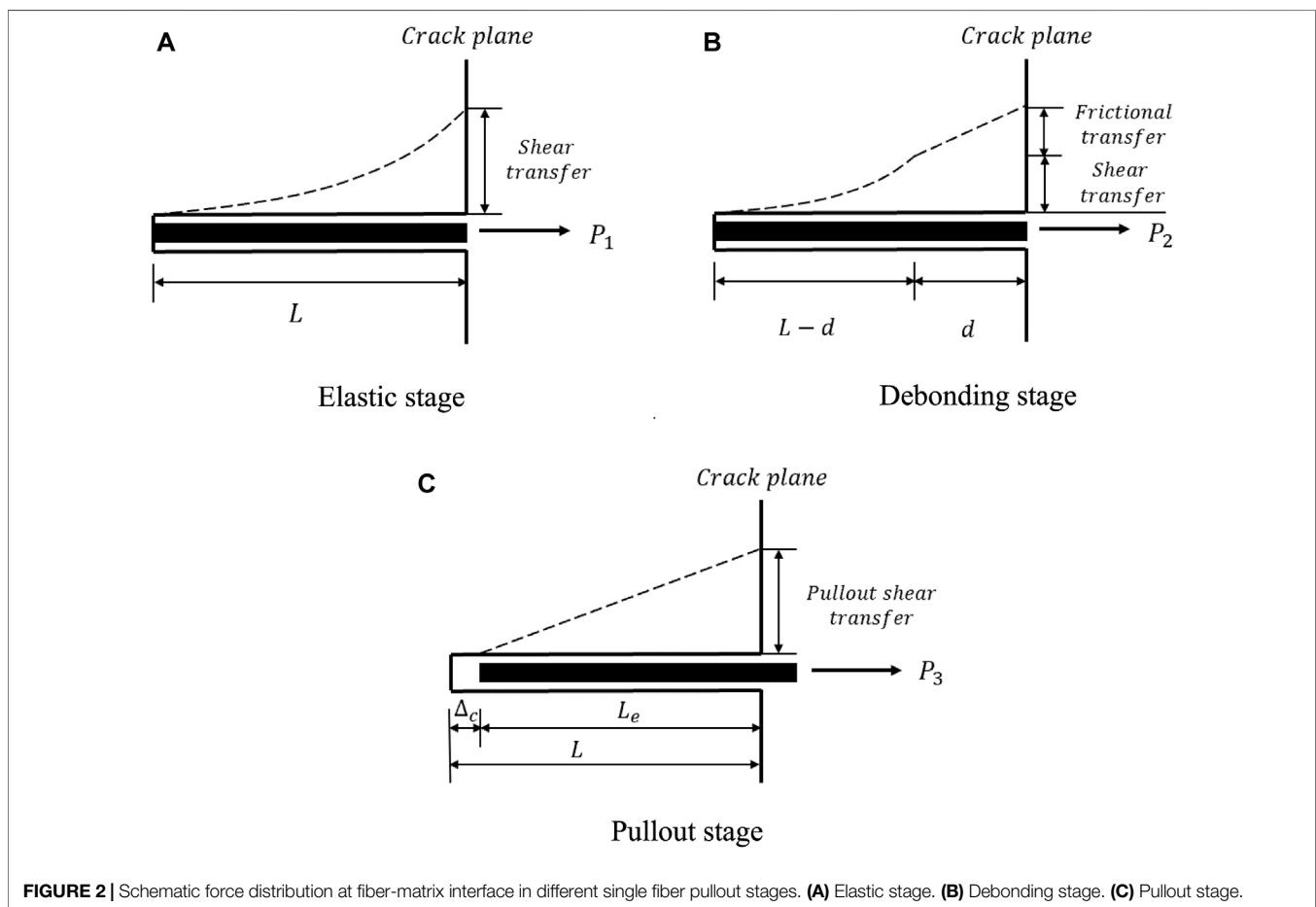
FIGURE 2 | Schematic force distribution at fiber-matrix interface in different single fiber pullout stages. **(A)** Elastic stage. **(B)** Debonding stage. **(C)** Pullout stage.

bridging constitutive law only considered the friction between fiber and matrix (Kanda and Li, 1998), new mechanisms of fiber/matrix interactions including slip hardening (Ochi et al., 2007), fiber rupture (Lin and Li, 1997), chemical bonding (Maalej et al., 1995) and two-way fiber debonding (Yang et al., 2008) were taken into account to improve the accuracy of crack opening prediction.

Above studies were mainly based on PVA fibers which exhibit high tenacity and good adhesion with cement. Flashbacking to the invention of SHCC in the 1990s, high-modulus polyethylene (PE) fibers were firstly used as the bridging fibers by Li et al. (Li, 1998), which are greatly more expensive than the other fibers. To reduce the high cost of fibers, SHCC with polyvinyl alcohol (PVA) fibers were introduced by

FIGURE 3 | Comparison between the experiment and existing model in the fiber pullout stage.
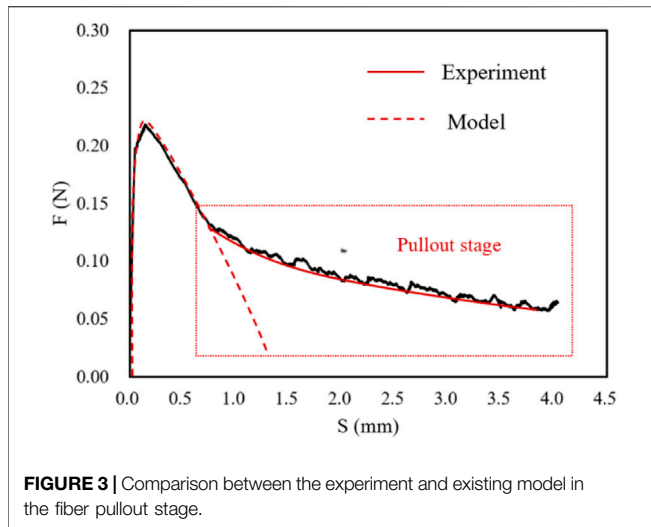
Kanda and Li (Kanda and Li, 1998). However, its application in construction is limited because the price is still relatively high for large-scale construction use (Pan et al., 2015). Therefore, cheaper substitute for PVA fibers is strongly in demand. By far, there have been many studies with other inexpensive synthetic fibers such as Polypropylene (PP) fibers, Polyacrylonitrile (PAN) fibers and polyethylene terephthalate (PET) fibers (Pereira et al., 2012; Pakravan et al., 2016; Lu et al., 2018; Zhigang, 2020b). The properties of different fibers vary widely, and even the same kind of fibers show completely different properties due to the different surface treatment processes (Foti, 2016), which directly results in differentiated performance of fibers when they are pulled out from the matrix. For example, PE and PVA fibers exhibit strong slip hardening characteristic (Li, 1998; Pan et al., 2015), while PAN and PET fibers show clear slip softening trend (Pereira et al., 2012; Lu et al., 2018). Therefore, it is not enough to establish a single fiber pullout model exclusively for PVA fibers. A unified model needs

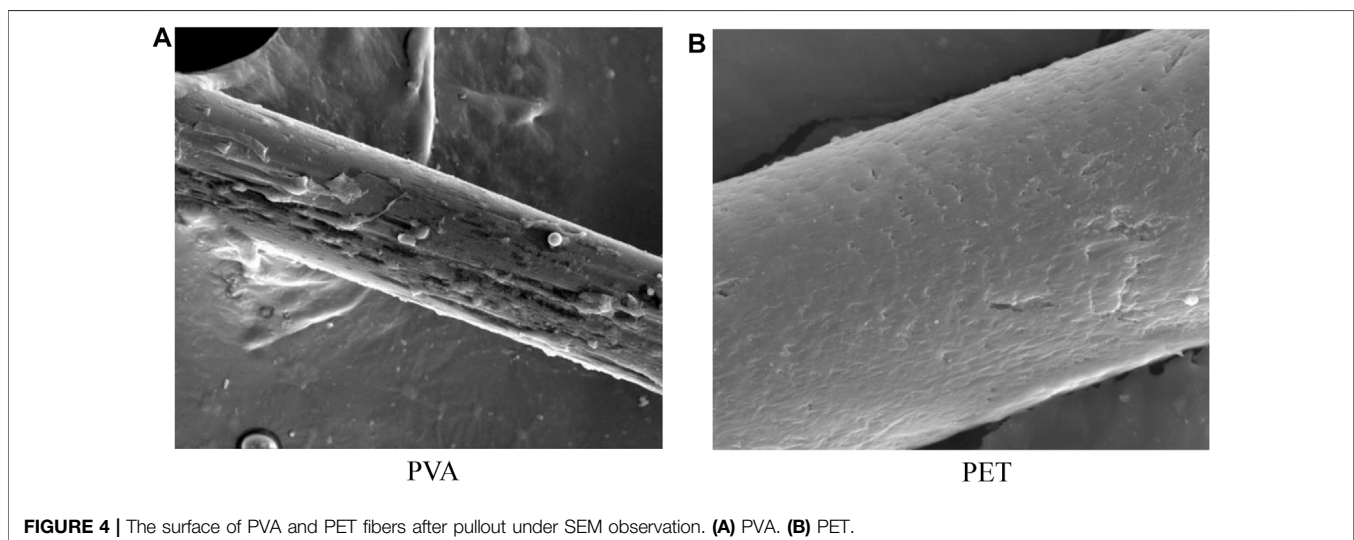to be developed to describe the single fiber pullout behavior of different fibers.

This paper aims at establishing a unified fiber bridging model of SHCC, applying to different kinds of fibers which may show different surface bonding properties. PVA fibers and PET fibers are taken as typical examples which show slip hardening and slip softening behavior, respectively. Modeling a single fiber pullout behavior against the surrounding matrix will be firstly conducted. Two new parameters including frictional strength during the pullout stage and the blocking length of fiber under pulley force are introduced to simulate the single fiber pullout behavior. In the following part, the stress-crack opening relation for a bridged crack is simulated based on the stochastic parameters derived from the single fiber pullout model. The revised fiber bridging model is then compared with the curve acquired from the experiment to confirm the validity.
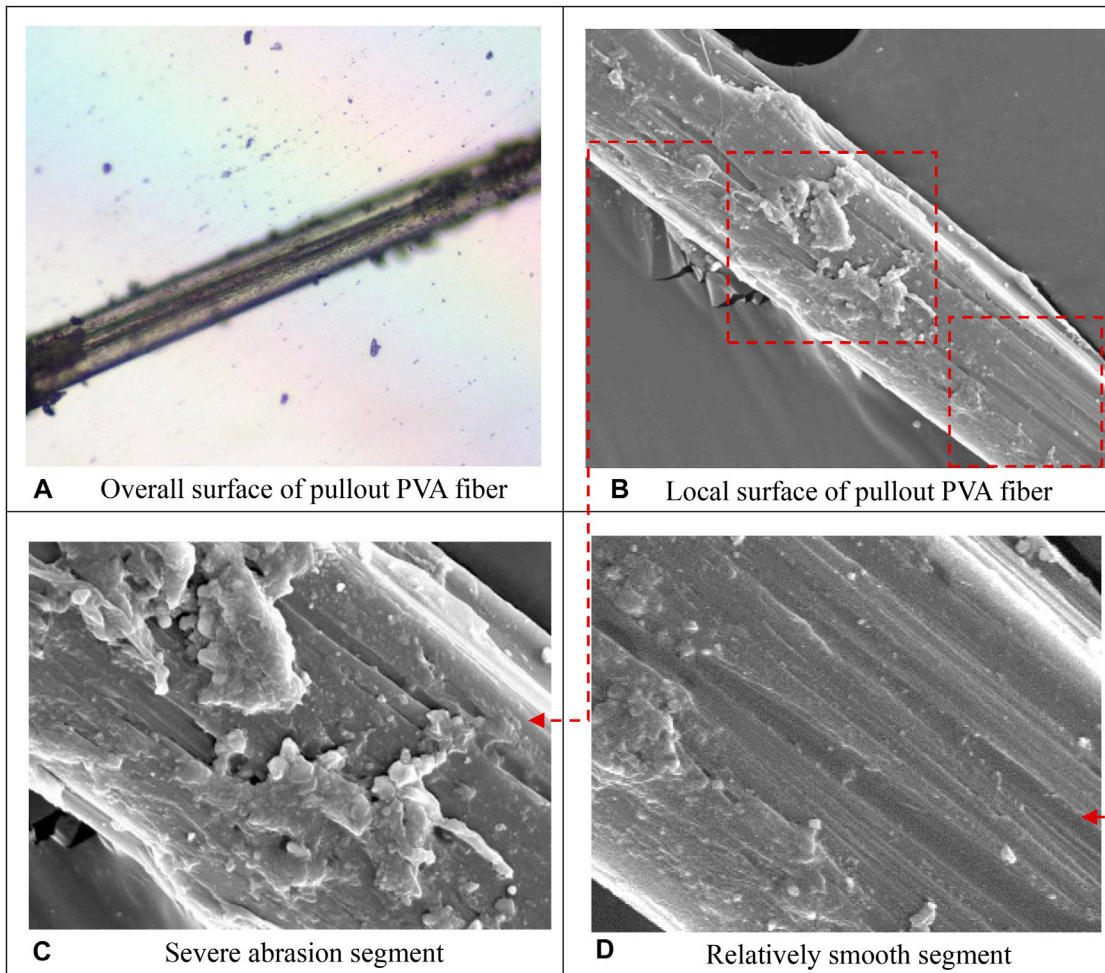
## MODELING OF SINGLE FIBER PULLOUT

Existing Theory

The pullout behavior of single fiber has been modelled in the literature (Lin and Li, 1997; Kanda and Li, 1999). In these existing models, when the fiber is subjected to a pullout force P, three stages are considered including elastic, debonding and pullout stage with different range of the slip S as shown in **Figure 1**. When the load is small, the local shear stress τ appears linear correlation with slip S and κ is the slope of the τ-S curve in elastic stage. When the shear stress exceeds the maximum shear strength τ_m, the debonding of the fiber is initiated and the frictional strength is defined as a constant value τ_d. After debonding reaches the embedded end of the fiber, the interface is purely governed by the frictional force and the fiber is assumed to be pulled out from the matrix, which is determined as pullout stage.

The model is established based on the static equilibrium requirement (Naaman et al., 1991; Li et al., 2003), and the tensile force in the fiber F is transferred to the matrix M

FIGURE 4 | The surface of PVA and PET fibers after pullout under SEM observation. **(A)** PVA. **(B)** PET.

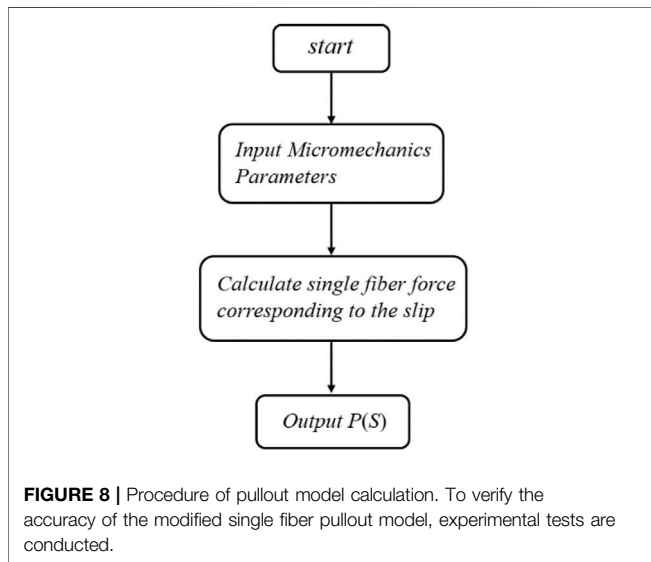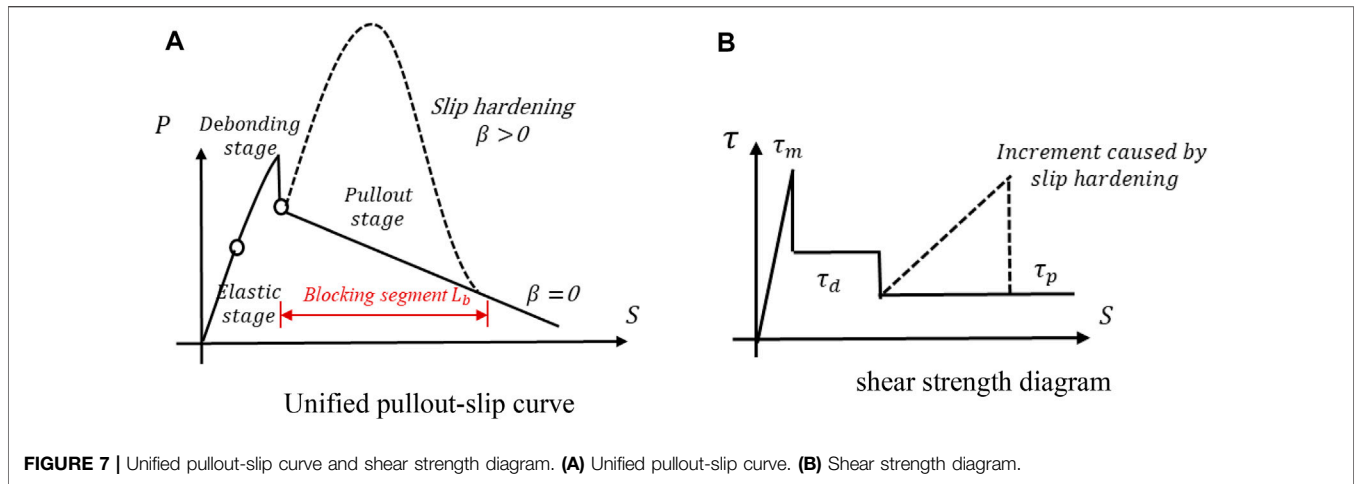**FIGURE 5 |** Various segments of the pullout PVA fiber surface under observation. **(A)** Overall surface of pullout PVA fiber. **(B)** Local surface of pullout PVA fiber. **(C)** Severe abrasion segment. **(D)** Relatively smooth segment.
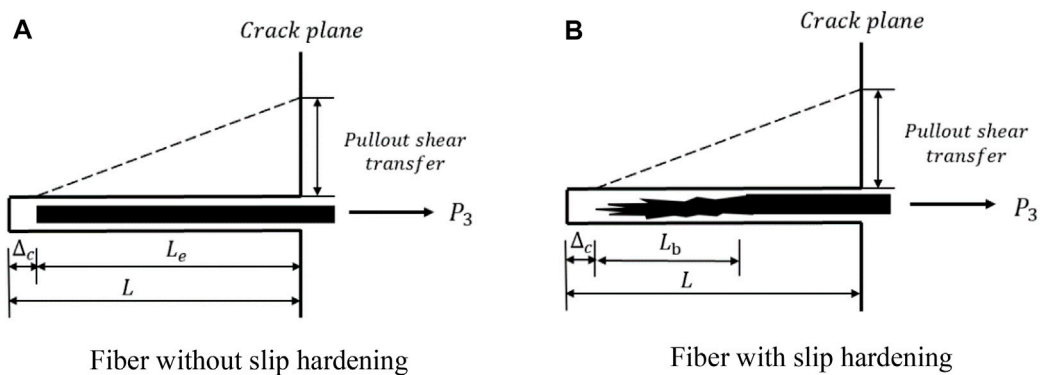
FIGURE 6 | Schematic diagram of introducing parameter blocking segment L_b into fiber pullout stage. **(A)** Fiber without slip hardening. **(B)** Fiber with slip hardening.

FIGURE 7 | Unified pullout-slip curve and shear strength diagram. **(A)** Unified pullout-slip curve. **(B)** Shear strength diagram.

FIGURE 8 | Procedure of pullout model calculation. To verify the accuracy of the modified single fiber pullout model, experimental tests are conducted.

TABLE 1 | Properties of fibers.

Fibers	Diameter (μ m)	Strength (MPa)	Modulus (GPa)
PVA	39	980	9.5
PET	20	900	6.0

The elastic modulus of the matrix is 20 GPa.

$$P_{1max} = \frac{\tau_m \psi}{\eta} \tanh(\eta L) \qquad (3)$$

When the shear stress exceeds the maximum shear strength τ_m, debonding for a length of d in **Figure 2B** is initiated, resulting in two separate regions, bonded and debonded. The shear strength of debonded stage decreases from τ_m to τ_d.

$$S_2 = \frac{P_{2max}Q}{\eta} \frac{\cosh(\eta(L-d)) - 1}{\sinh(\eta(L-d))} + \frac{1}{2}Qd(\tau_d\psi d + 2P_{2max}) \quad (4)$$

$$P_{2max} = \frac{\tau_m \psi}{\eta} tanh(\eta(L-d)) \qquad (5)$$

It is assumed that at the time the fiber is completely debonded, the shear resistance still remains τ_d, leading to a simplified rigid body motion after sliding begins ($\Delta c > 0$) as shown in **Figure 2C**.

$$S_3 = -\frac{\tau_d\psi Q}{2}(L - \Delta c)^2 + P_{3,nth}Q(L - \Delta c) \qquad (6)$$

$$P_3 = \tau_d\psi(L - \Delta c) \qquad (7)$$

New Considerations in Single Fiber Pullout Stage

The above section illustrates the stress transfer via interface between the fiber and matrix when the fiber is being pulled out. However, due to the great divergency in the interface properties between various fibers, the previous model mentioned above cannot apply to different types of fibers. The limitations will be explained in detail in this section.

through the interface. This relationship expressed in the differential form is

$$\frac{dF}{dx} = -\frac{dM}{dx} = \psi\tau \qquad (1)$$

where ψ = equivalent circumference of the fiber; and τ = shear stress at fiber-matrix interface.

When the fiber and matrix are fully bonded as shown in **Figure 2A**, the relationship between slip S_1 and the bonded load P_1 can be formulized as
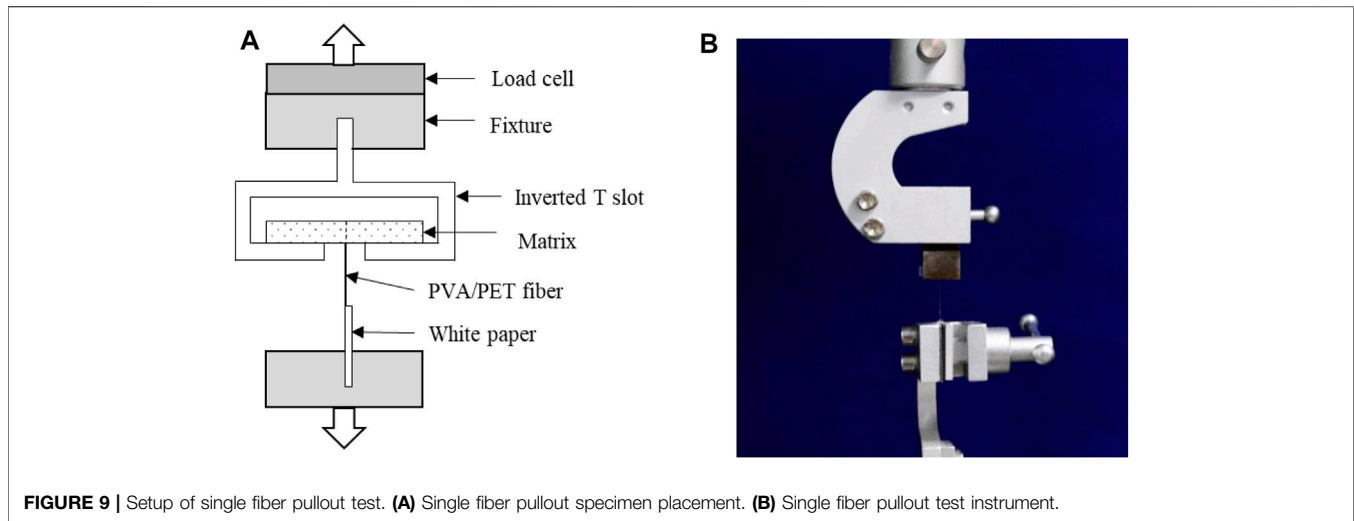
$$S_1 = \frac{P_1 Q}{\eta \sinh(\eta L)} [cosh(\eta L) - 1] \qquad (2)$$

where $\eta^2 = \psi\kappa Q$ and slope κ is defined from the shear strength diagram, $Q = \frac{1}{A_y E_y} + \frac{1}{A_m E_m}$. When shear stress at x = L reaches the maximum strength, the elastic stage is terminated and the maximum bonded load is calculated by

FIGURE 9 | Setup of single fiber pullout test. **(A)** Single fiber pullout specimen placement. **(B)** Single fiber pullout test instrument.

TABLE 2 | interfacial parameters for PVA and PET fiber pullout simulation.

PVA/No	τ_m (MPa)	τ_d (MPa)	τ_p (MPa)	L_b (mm)	β	PET/No	τ_m (MPa)	τ_d (MPa)	τ_p (MPa)	L_b (mm)	β
1	1.20	0.55	0.32	1.70	0.20	1	0.80	0.52	0.36	0	0
2	0.90	0.60	0.34	1.5	0.32	2	0.65	0.50	0.30	0	0
3	0.80	0.70	0.38	1.50	0.34	3	1.15	0.60	0.36	0	0
4	0.90	0.90	0.30	2.20	0.45	4	0.95	0.65	0.46	0	0
5	0.95	0.90	0.33	2.60	0.48	5	0.80	0.70	0.36	0	0
6	0.90	0.90	0.32	2.20	0.46	6	0.80	0.58	0.38	0	0
7	1.10	1.10	0.40	2.50	0.46	7	1.05	0.70	0.42	0	0
8	1.10	1.10	0.51	1.90	0.5	8	1.10	0.85	0.58	0	0
9	1.40	1.20	0.95	1.90	0.16	9	0.90	0.73	0.52	0	0
10	0.90	0.85	0.75	2.00	0.22	10	1.20	1.10	0.70	0	0
11	1.30	1.20	0.90	1.95	0.28	11	1.15	1.05	0.80	0	0
12	1.10	1.00	0.65	2.20	0.22	12	1.20	1.10	0.70	0	0
13	1.60	1.40	0.50	1.56	0.43	13	0.90	0.85	0.48	0	0
14	1.60	1.50	0.60	1.45	0.37	14	1.00	0.93	0.62	0	0
15	1.40	1.30	0.50	1.55	0.45	15	1.20	1.10	0.60	0	0
16	1.10	1.00	0.50	1.30	0.52	16	0.80	0.73	0.50	0	0

Limitation 1: Inconsistency of Frictional Strength During Different Fiber Pullout Stages

According to the above assumption, the frictional strength used in the debonding and pullout stages is the same parameter τ_d shown in **Figure 1**. Nevertheless, this assumption is not completely consistent with the actual situation. As is shown in **Figure 3**, it is assumed that at the time the fiber is completely debonded, the shear resistance still remains τ_d in the previous model. However, in the experiment the force in the pullout stage descends at a slower rate compared to that in the debonding stage, which should be related to the difference of the static friction and dynamic friction (Sueki et al., 2007) Therefore, it is necessary to adopt different frictional strength in different stages according to the actual pullout situation.

Limitation 2: Varying Slipping Behaviors for Different Fibers

In the actual experimental observation, slipping behaviors for different fibers vary widely due to the completely different interfacial properties between the matrix and the fibers. The possible slipping phenomena in the fiber pullout stage are compared between the PVA and PET fiber. When the PVA fibers slide along the interface tunnel between fiber and matrix, the pullout force suddenly increases due to abrasion and jamming. By scanning electron microscope (SEM), it can be seen that the surface of PVA fiber (**Figure 4A**) has serious abrasion, while the surface of PET fiber (**Figure 4B**) is relatively smooth after pullout from the matrix. Hence, the various pullout performance of PET and PVA due to the different surface properties of fibers should be considered.

Limitation 3: Partial Abrasion Surface of Single Fiber After Pullout

Moreover, by Scanning Electron Microscope (SEM) shown in **Figure 5**, the PVA fiber showed both severe abrasion and relatively smooth segments after pullout, indicating that only part of the fiber was worn during pullout stage. Therefore, the partial blocking segment should be introduced to simulate the actual pullout
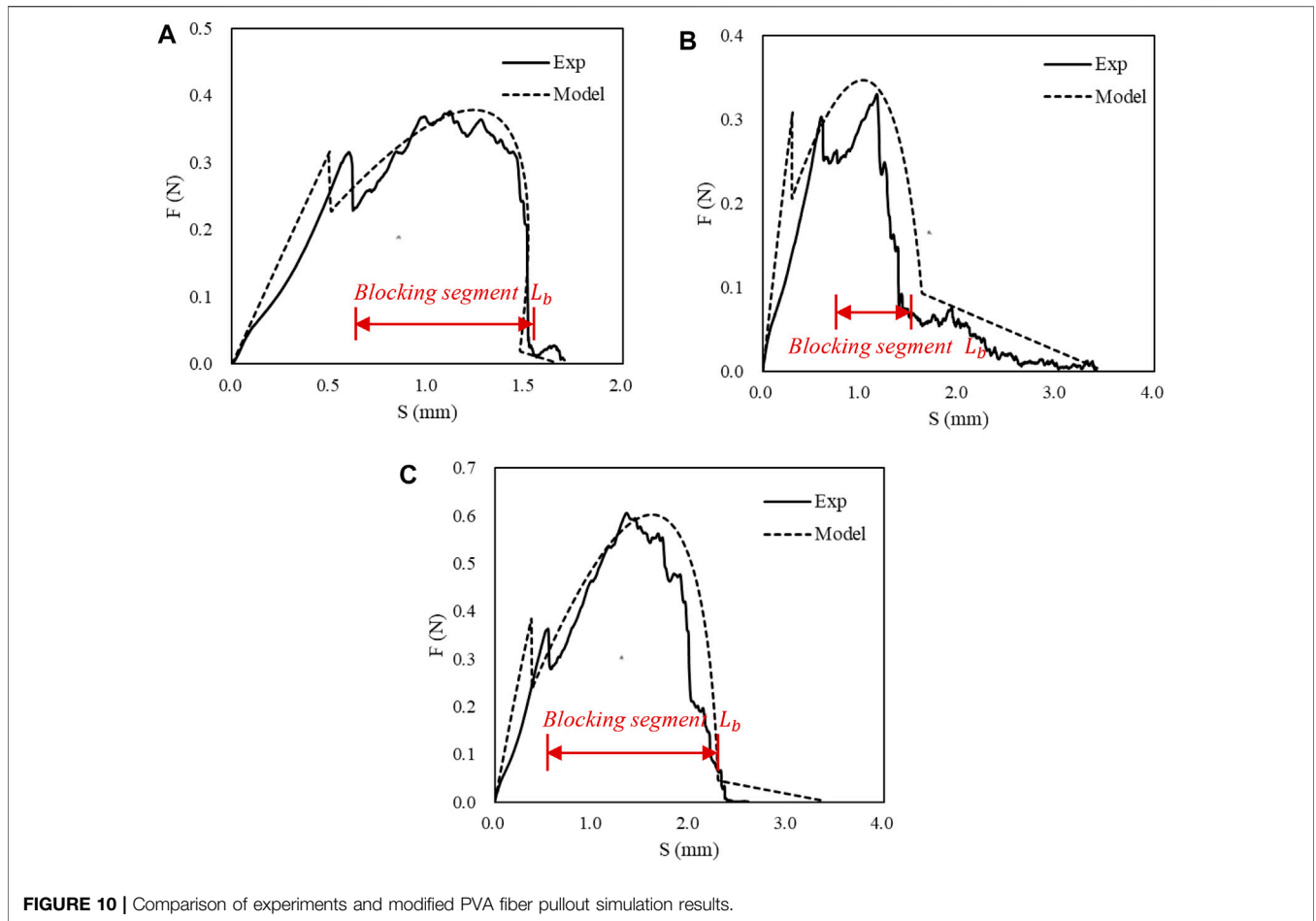
FIGURE 10 | Comparison of experiments and modified PVA fiber pullout simulation results.

process compared with the sliding hardening coefficient applied to the whole pullout process in the previous study (Yang et al., 2008).

Refined Single Fiber Pullout Model With New Considerations

To address the mentioned limitations of current model, a refined model for single fiber pullout is proposed in this section.

As mentioned before, the frictional strength varies in different fiber pullout stages, especially in the debonding and pullout stages. To account for this variation, a new parameter pullout frictional strength τ_p is adopted. During the fiber pullout process, fiber and matrix are fully bonded when the shear stress at interface is less than the maximum chemical strength τ_m. Along the debonded zone the frictional strength is constant as τ_d. Sliding begins right after the completion of debonding and the resisting frictional strength is assumed to drop to pullout strength τ_p. By introducing this new parameter, the overall trend of pullout stage will be flatter and more consistent with the experiment than the previous model.

Moreover, considering the surface of some fibers bonded with the matrix is partly worn under pulley force which results in obvious slip hardening phenomenon, the new parameter blocking segment L_b (as shown in **Figure 6**) and is introduced to describe different slipping phenomena.

The pulley force of fiber with slip hardening in the pullout stage can be expressed as

$$P_3 = \tau_p \left[(L_b - \Delta_d + \Delta_c)\left(1 + \frac{\beta(\Delta_d - \Delta_c)}{D}\right) + (L + \Delta_c - L_b) \right] \tag{8}$$

where, Δ_d represents the fiber displacement, slip hardening coefficient β represents the rate of frictional change, Δ_c represents the debonding length, and D represents fiber diameter.

By adding these new parameters, the fiber like PVA fiber which has obvious slip hardening phenomenon can be simulated more accurately, and the pullout phenomena of fibers with different properties can be unified through the processing of the pullout stage formula as shown in **Figure 7**.

Based on the analytical model established above, the curves obtained from the experiment can be simulated. The specific calculation process is summarized as follows in **Figure 8**.

Experimental Validation

In this section, the preparation and setup of single fiber pullout tests are introduced in detail. Moreover, parameters are fitted based on different experimental curves to obtain more accurate fiber bridging curve.
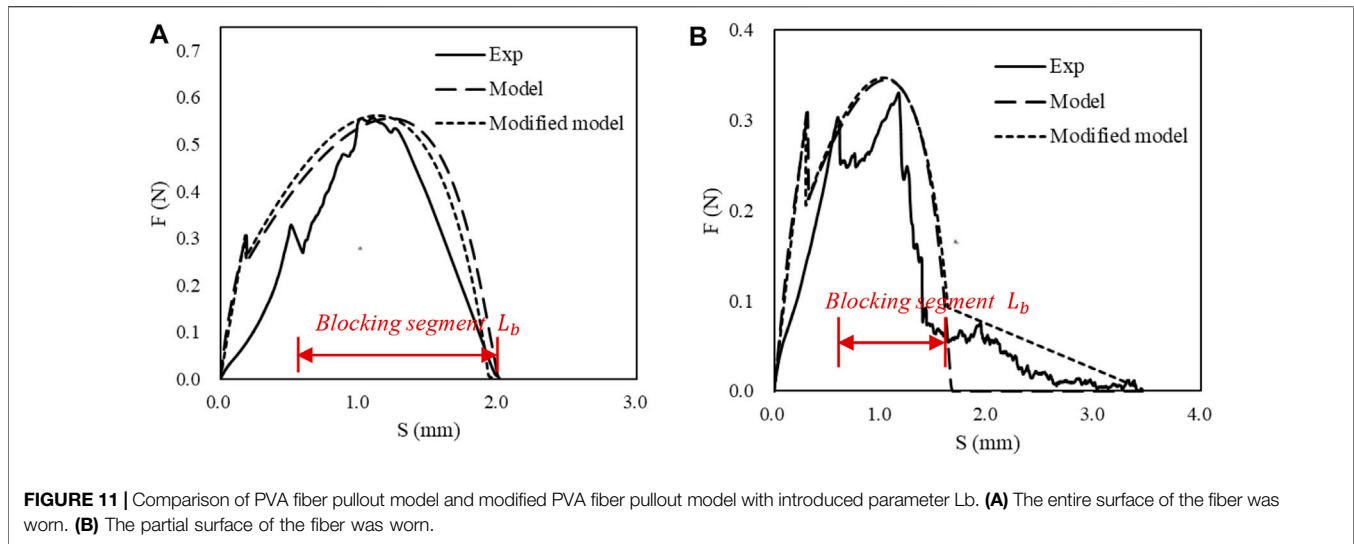
FIGURE 11 | Comparison of PVA fiber pullout model and modified PVA fiber pullout model with introduced parameter Lb. **(A)** The entire surface of the fiber was worn. **(B)** The partial surface of the fiber was worn.

Setup of Single Fiber Pullout Test

The main components of SHCC matrix materials used in the test are ordinary silicate 42.5 cement, F class I level fly ash, 80–100 mesh quartz sand and polycarboxylic acid water-reducing agent (PCA).

The fibers selected in the test are PET fiber and domestic PVA fiber. According to the actual measurement, the basic mechanical parameters are shown in **Table 1**.

Single fiber pullout test was performed to evaluate the interfacial bond between the PVA/PET fiber and the matrix. Then the experimental curve was fitted, respectively, to obtain the fitting parameters. In this test, the testing setup is shown in **Figure 9**. More details of the test can be found in Katz and Li (1996). As shown in **Figure 9A**, the fiber pullout specimen was placed on an inverted T slot. At the same time, the free end of PVA/PET fiber was glued to a piece of white paper, which was fixed with the lower fixture. The single fiber was pulled out under displacement control at the rate of 0.5 mm/min.

Results and Discussion on the Single Fiber Pullout Test

Simulation of single fiber pullout based on the new model is conducted on each individual tested specimen. The parameters including $\tau_m, \tau_d, \tau_p, L_b$ and β are estimated in order to find a match between the simulation and experiment. Nominal shear strength τ_n has been defined to estimate the value of τ_m and τ_d.

$$\tau_n = \frac{F_{max}}{\pi D L} \tag{8a}$$

where F_{max} = maximum load of experiment; D = diameter of a fiber; and L = embedded length of fiber.

τ_m controls the development rate of elastic stage, the value of which is higher than that of τ_n. τ_d is related to the maximum force of the debonding stage, the value of which tend to be lower

than that of τ_n. τ_p controls the development rate of pullout stage and its value is the minimum.

L_b and β are used to describe slip hardening phenomenon. L_b is obtained by calculating the difference between displacement at the end of slip hardening and that at the beginning of slip hardening. Based on the determined L_b, higher value of β means higher value of second peak. The parameters used for all specimens are listed in **Table 2** below.

It can be seen that in the PVA fiber pullout stage, the blocking segment for each fiber in **Figure 10** vary from each other, while the modified model can simulate well regardless of the length of the blocking segment. The modified model is consistent with the test results which show various lengths of blocking segment L_b. This proves that the introduction of new parameters can simulate the real situation more properly.

The previous model and the modified model both can fit well with the experimental curve when the entire surface of the fiber was worn under pulley force as shown in **Figure 11A**. However, when the surface of the fiber was partially worn, the previous model could not fit well with the experimental curve in the pullout stage. With the introduced parameter L_b, the modified single fiber pullout model can apply to the same fibers which show various lengths of blocking segment under pulley force.

Compared with PVA fibers which have obvious blocking segment, PET fibers show negligible slip-hardening in **Figure 12**. This difference is expected since the surface of PET fiber is smoother than that of the PVA fiber.

Overall, the proposed single fiber pullout model can fit well with the experimental results for both the PVA and PET fibers. It can be seen that different parameters derived from the pullout tests vary widely between different fibers in **Table 2**. Therefore, normal distribution is conducted based on the obtained parameters to better describe the stochasticity of fiber pullout characteristic.

FIGURE 12 | Comparison of experiments and modified PET fiber pullout simulation results.
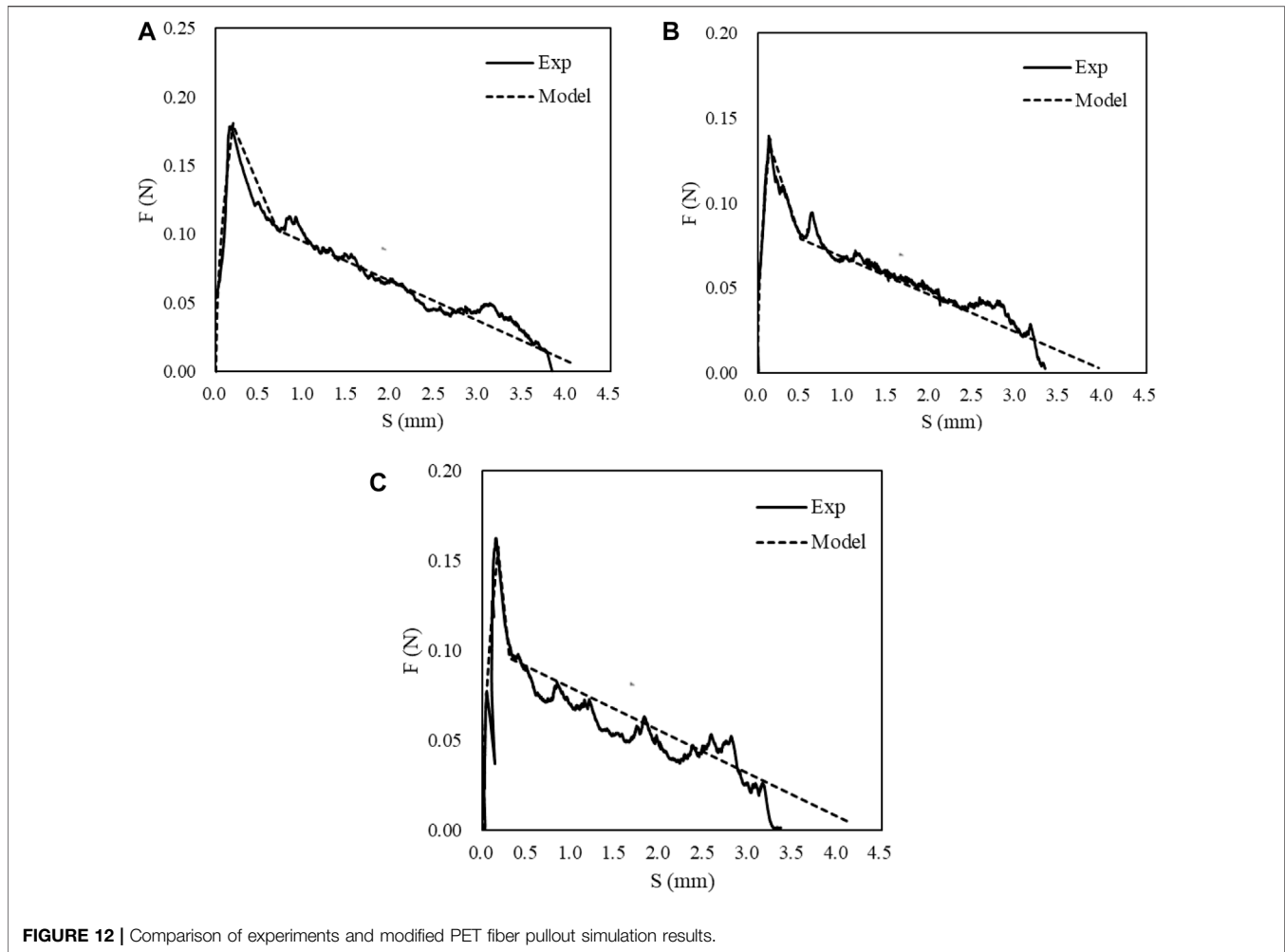
MODELING OF FIBER-BRIDGING CONSTITUTIVE LAW σ(δ)

Description of the Stochasticity in the Fiber Pullout Behaviors

According to the parameter results obtained from single fiber pullout simulation above, even the same kind of fibers vary a lot in discreteness. Considering such difference, average values were used in the previous study to apply these parameters to a larger scale like simulation of fiber bridging curve. However, the randomness of interface parameters cannot be expressed completely by using the average values, so the parameters used in fiber bridging curve are obtained from normal distribution in this paper.

As illustrated in **Figure 13**, all parameters were randomized for PVA and PET fibers, respectively. Then a modified single crack model will be established based on the parameters

selected randomly from the probability distribution of these parameters.

Modeling Strategy of the σ(δ) Relation for Single Crack

Fiber-bridging constitutive law σ(δ) describes the relationship between the bridging stress σ transferred across a crack and the opening of this crack δ. On the one hand, this curve is related to the material microstructure. On the other hand, tensile strain-hardening behavior of composites is governed by this law. Therefore, to successfully design SHCC material properties, it is necessary to understand and simulate the σ(δ) curve with good accuracy.

For a fiber perpendicular to the interface between fiber and matrix, the parameters are selected randomly from the probability distribution of these parameters above in **Figure 13**. Therefore, a
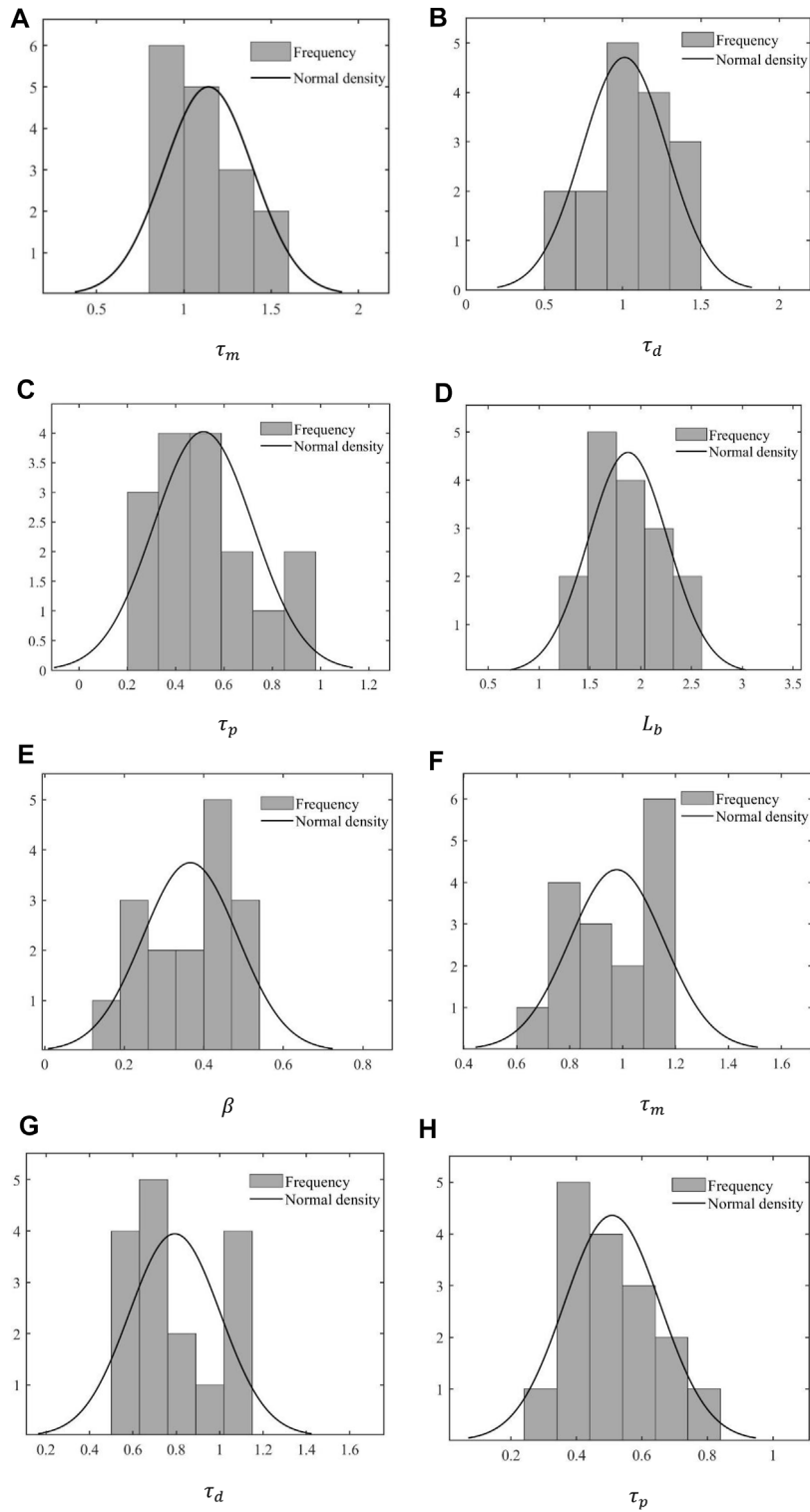
FIGURE 13 | Histogram of normal distribution: **(A–E)** in PVA fiber, **(F–H)** in PET fiber.
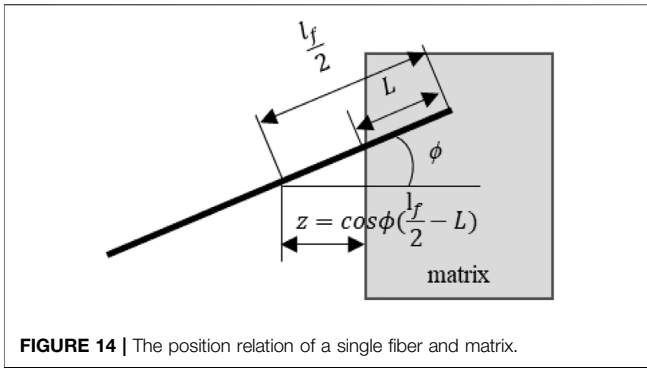
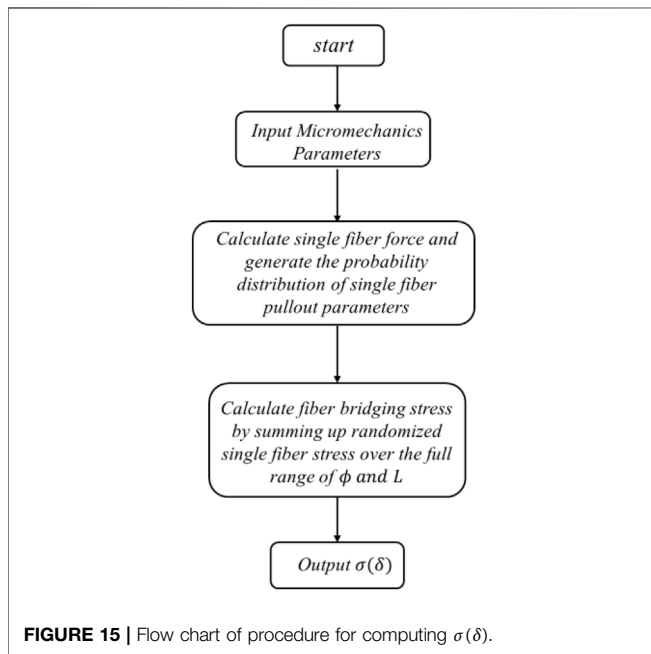**FIGURE 14 |** The position relation of a single fiber and matrix.

FIGURE 15 | Flow chart of procedure for computing $\sigma(\delta)$.

FIGURE 16 | Dimensions of single crack tensile specimen (mm).

FIGURE 17 | Setup of single crack test.

single fiber pullout force can be calculated when the orientation angle ϕ is 0. However, the bridging force is contributed by the fibers which are randomly distributed with different orientation angle ϕ and embedding length L. Hence, the fiber-bridging $\sigma(\delta)$ relation is available through assuming the force of fibers with different centroidal distance z and orientation angle ϕ on the crack plane. The position relation of a single fiber and matrix is shown in **Figure 14**.

Equation 9 shows the formulation of fiber-bridging $\sigma(\delta)$ relation.

$$\sigma(\delta) = \frac{1}{A_f V_f} \int P(z,\phi) p(z,\phi) dz d\phi \qquad (9)$$

A_f and V_f are the cross-sectional area and volume fraction of fiber, respectively. $P(z,\phi)$ is the bridging force contributed by a single fiber with distance z and orientation angle ϕ. $p(z,\phi)$ is the probability density function of fiber with distance z and orientation angle ϕ.
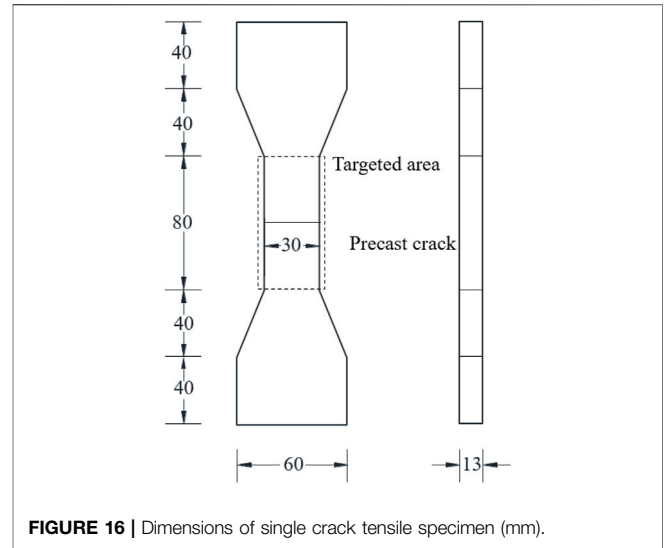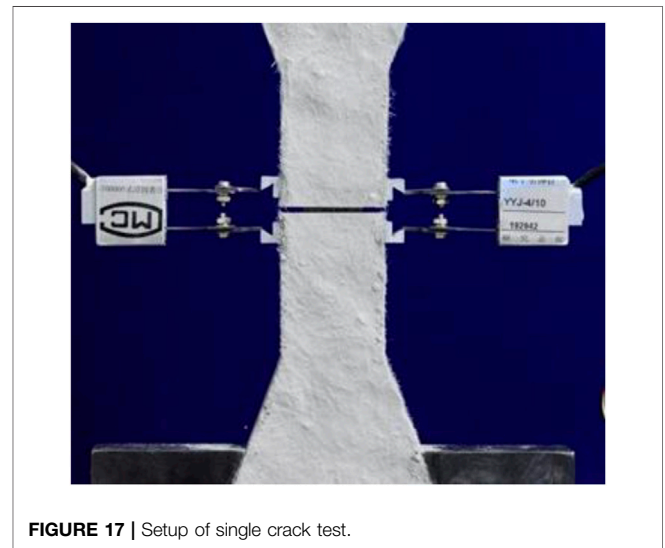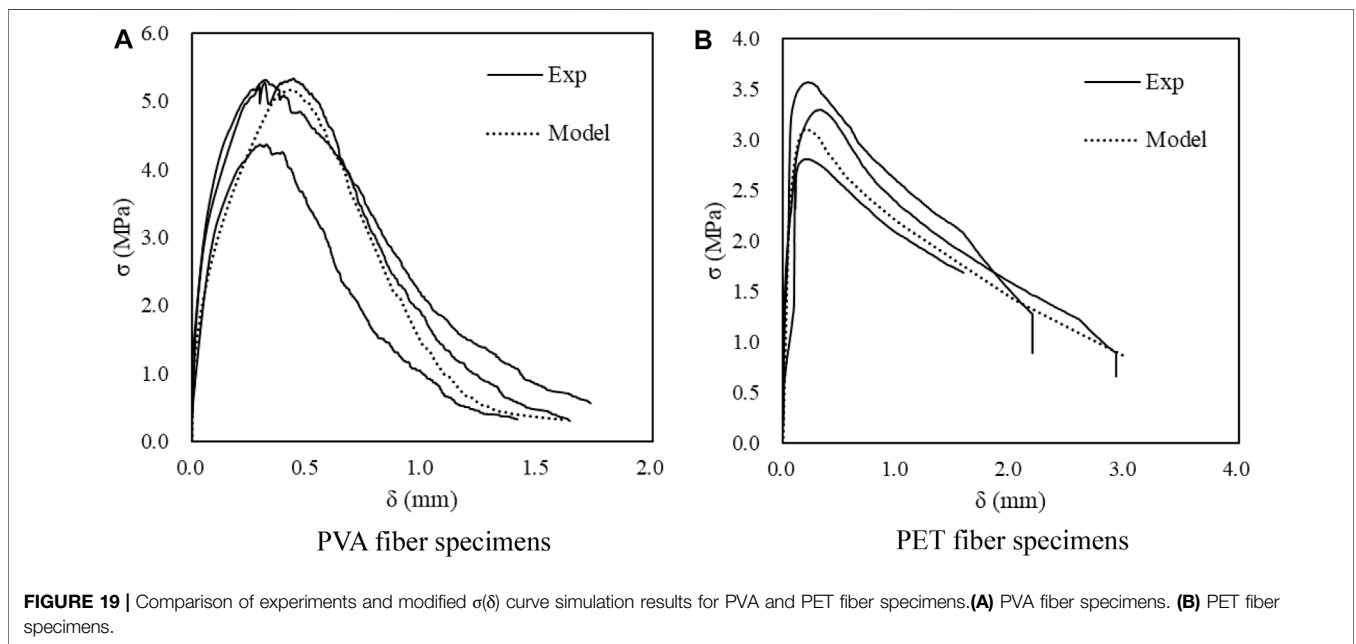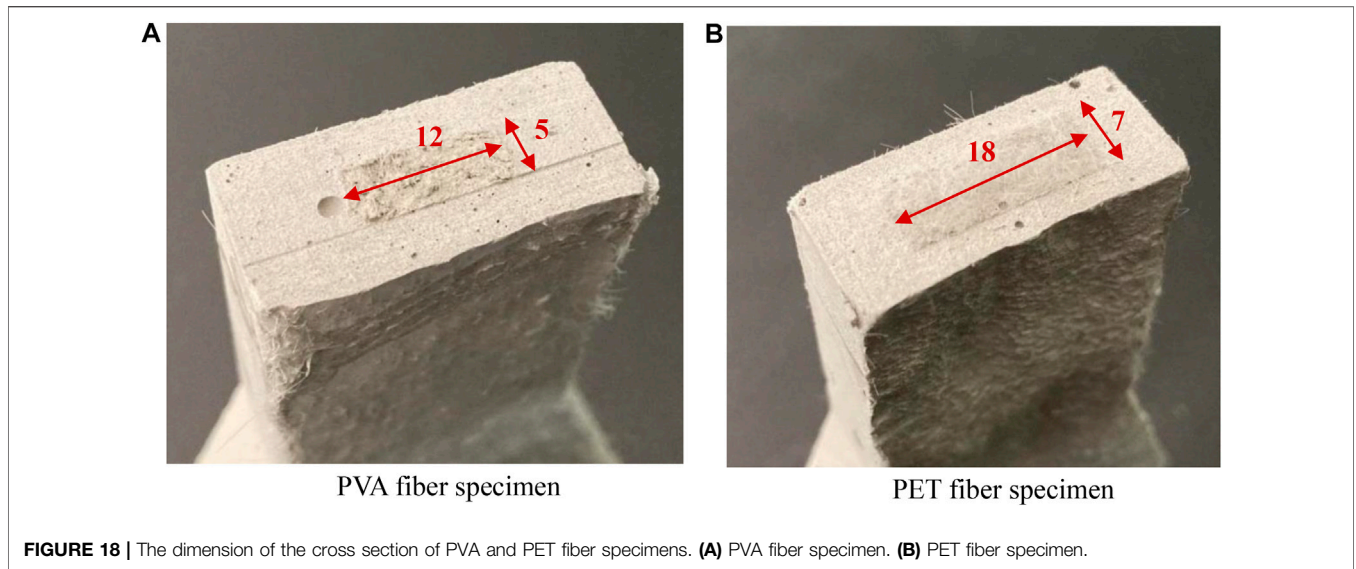
The probability density functions of distance z and orientation angle ϕ are independent of each other. So $p(z,\phi)$ can be expressed as following

$$p(z,\phi) = p(z)p(\phi) \qquad (10)$$

$$p(z) = \frac{2}{l_f}, 0 \leq z \leq \frac{l_f}{2} \qquad (11)$$

$$p(\phi) = \sin(\phi), 0 \leq \phi \leq \frac{\pi}{2} \qquad (12)$$

A discrete method was adopted to deal with such complex analytic expressions in previous studies (Lu and Leung, 2016), which divides the fibers according to the combination of their inclination and embedding length. Assuming that the fibers are randomly distributed, fibers with different embedment length are uniformly divided into 100 groups from 0 to $L/2$, and those at different inclination angles are divided into 100 groups from 0 to $\pi/2$. Hence, 10,000 different groups are

FIGURE 18 | The dimension of the cross section of PVA and PET fiber specimens. **(A)** PVA fiber specimen. **(B)** PET fiber specimen.

FIGURE 19 | Comparison of experiments and modified σ(δ) curve simulation results for PVA and PET fiber specimens. **(A)** PVA fiber specimens. **(B)** PET fiber specimens.

considered totally. Meanwhile, assuming that fibers with longer embedment length (from $L/2$ to L) have the same distribution as fibers with shorter embedment length and their lengths sum up to L. Therefore, when calculating the friction transfer with a certain embedment length, the frictional stress from both the long and short embedment side should be calculated and averaged.

Through this way, the stress-crack opening curves are simulated and compared with the experimental results. The specific calculation process is summarized in **Figure 15**.

Verification With Experimental Results

Single crack tensile test was conducted to compare with the simulation results. Dog-bone specimen is used according to the SHCC mechanical test specification, and the specific size is shown in **Figure 16**.

The test preparation is shown in **Figure 17**. The preparation of specimens mainly includes weighing, mixing, pouring, demolding and curing of raw materials. After curing, the middle section of the specimen was notched by a cutting

machine to prevent the phenomenon of multi-crack cracking during tensile test and the dimension of the cross section of PVA and PET fiber specimens are shown in **Figure 18**. For the test setup, the edge of electronic extensometer was glued on the side of the specimen, and the force arm of the extensometer was finally clamped and fixed on the tool edge.

It can be seen in **Figure 19** that the bridging stress reaches the peak stress at roughly 5 MPa in PVA fibers while PET fibers can only reach 3 MPa peak stress. Besides the peak bridging stress, the corresponding crack opening displacement δ for PVA fiber specimen is wider than that for PET fiber specimen, which means that PVA fibers may have better ductility. Meanwhile, due to the larger crack width, the durability of PVA fiber specimen may be not as good. Compared with the PVA fiber specimen, PET fibers can continue to bridge the matrix under a larger crack opening displacement more than 2 mm. It is likely due to the interfacial bond between PVA fiber and the matrix is stronger than that between PET fiber and the matrix. Due to the weaker bond with the matrix, PET fiber shows higher tendency to pull out, which accounts for the flatter decline trend of PET fiber in the pullout stage as shown in **Figure 19B**.

Overall, the single crack model which is built based on the proposed single fiber pullout model fits well with the test results so the validity is confirmed again.

CONCLUSION

In this study, a unified model for single fiber pullout was successfully developed with introduced parameters, which is suitable for fibers with different interfacial properties, including PET and PVA fibers investigated in this paper. Single crack model based on the new single fiber pullout model was then developed, which takes into account the stochasticity of various pullout behaviors between different fibers. Experimental verification on single fiber pullout and single crack opening were conducted to show that the proposed model can agree well with the test results.

To conclude, this model is suitable not only for one specific fiber, but can apply to different kinds of fibers by one united form, which was verified by experiments in PVA and PET fiber systems. This revised fiber-bridging model can be utilized to predict the composite tensile ductility of SHCC with different fibers effectively, which will help the understanding and micro-mechanics-based design of SHCC materials.

DATA AVAILABILITY STATEMENT

The original contributions presented in the study are included in the article/Supplementary Material, further inquiries can be directed to the corresponding author.

AUTHOR CONTRIBUTIONS

PS was responsible for most experimental testing and model simulation work, CL put forward constructive suggestions for the revision of this paper, JW assisted in the simulation of single crack model and ZP offered help to scan the specimen by SEM.

REFERENCES

Foti, D. (2016). Innovative Techniques for concrete Reinforcement with Polymers. *Construction Building Mater.* 112, 202–209. doi:10.1016/j.conbuildmat.2016.02.111

Graybeal, B. A. (2006). *Material Property Characterization of Ultra-high Performance concrete Creep.*

Jun, Z., Leung, C. K. Y., and Yin Nee, C. (2006). Flexural Performance of Layered ECC-concrete Composite Beam. *Composites Sci. Technol.* 66 (11-12), 1501. doi:10.1016/j.compscitech.2005.11.024

Kanda, T., and Li, V. C. (1999). Effect of Fiber Strength and Fiber-Matrix Interface on Crack Bridging in Cement Composites. *J. Eng. Mech.* 125 (3), 290–299. doi:10.1061/(asce)0733-9399(1999)125:3(290)

Kanda, T., and Li, V. C. (1998). Interface Property and Apparent Strength of High-Strength Hydrophilic Fiber in Cement Matrix. *J. Mater. civil Eng.* 10 (1), 5–13. doi:10.1061/(asce)0899-1561(1998)10:1(5)

Katz, A., and Li, V. C. (1996). A Special Technique for Determining the Bond Strength of Micro-fibres in Cement Matrix by Pullout Test. *J. Mater. Sci. Lett.* 15 (20), 1821–1823. doi:10.1007/bf00275353

Leung, C. K. Y. (1996). Design Criteria for Pseudoductile Fiber-Reinforced Composites. *J. Eng. Mech.* 122 (1), 10–18. doi:10.1061/(asce)0733-9399(1996)122:1(10)

Li, V. C. (1998). Engineered Cementitious Composites - Tailored Composites through Micromechanical Modeling. *J. Adv. Concrete Techn.* 1(3).

Li, V. C. (2011). *Engineered Cementitious Composites (ECC) – Material, Structural, and Durability Performance.*

Li, V. C., Mishra, D. K., Naaman, A. E., Wight, J. K., and Inada, Y. (2003). On the Shear Behavior of Engineered Cementitious Composites. *Adv. Cement Based Mater.* 1 (3), 142. doi:10.1016/1065-7355(94)90045-0

Li, V. C. (2012). On Engineered Cementitious Composites (ECC) A Review of the Material and its Applications. *Fiber reinforced Concrete Engineering Materials 2012 Summit Forum of China Association of Concrete and Cement Products*, 2164, 1-810.

Li, V. C., Wang, S., and Wu, C. (2001). Tensile Strain-Hardening Behavior of Polyvinyl Alcohol Engineered Cementitious composite(PVA-ECC). *Aci Mater. J. 98(6)*, 483.

Li, V. C., and Leung, C. K. Y. (1992). Steady-State and Multiple Cracking of Short Random Fiber Composites. *J. Eng. Mech.* 118 (11), 2246–2264. doi:10.1061/(asce)0733-9399(1992)118:11(2246)

Li, V. C., and Wu, H.-C. (1992). Conditions for Pseudo Strain-Hardening in Fiber Reinforced Brittle Matrix Composites. *Appl. Mech. Rev.* 45 (8), 390–398. doi:10.1115/1.3119767

Lin, Z., and Li, V. C. (1997). Crack Bridging in Fiber Reinforced Cementitious Composites with Slip-Hardening Interfaces. *J. Mech. Phys. Sol.* 45 (5), 763–787. doi:10.1016/s0022-5096(96)00095-6

Lu, C., and Leung, C. K. Y. (2016). A New Model for the Cracking Process and Tensile Ductility of Strain Hardening Cementitious Composites (SHCC). *Cement Concrete Res.* 79, 353–365. doi:10.1016/j.cemconres.2015.10.009

Lu, C., Yu, J., and Leung, C. K. Y. (2018). Tensile Performance and Impact Resistance of Strain Hardening Cementitious Composites (SHCC) with Recycled Fibers. *Construction Building Mater.* 171, 566–576. doi:10.1016/j.conbuildmat.2018.03.108

Maalej, M., Li, V. C., and Hashida, T. (1995). Effect of Fiber Rupture on Tensile Properties of Short Fiber Composites. *J. Eng. Mech.* 121 (8), 903–913. doi:10.1061/(asce)0733-9399(1995)121:8(903)

Naaman, A. E., Namur, G. G., Alwan, J. M., and Najm, H. S. (1991). Fiber Pullout and Bond Slip. I: Analytical Study. *J. Struct. Eng.* 117.

Ochi, T., Okubo, S., and Fukui, K. (2007). Development of Recycled PET Fiber and its Application as concrete-reinforcing Fiber. *Cement and Concrete Composites* 29 (6), 448–455. doi:10.1016/j.cemconcomp.2007.02.002

Pakravan, H. R., Latifi, M., and Jamshidi, M. (2016). Ductility Improvement of Cementitious Composites Reinforced with Polyvinyl Alcohol-Polypropylene Hybrid Fibers. *J. Ind. Textiles* 45 (5), 637–651. doi:10.1177/1528083714534712

Pan, Z., Wu, C., Liu, J., Wang, W., and Liu, J. (2015). Study on Mechanical Properties of Cost-Effective Polyvinyl Alcohol Engineered Cementitious Composites (PVA-ECC). *Construction Building Mater.* 78, 397–404. doi:10.1016/j.conbuildmat.2014.12.071

Pereira, E. B., Fischer, G., and Barros, J. A. O. (2012). Effect of Hybrid Fiber Reinforcement on the Cracking Process in Fiber Reinforced Cementitious Composites. *Cement and Concrete Composites* 34 (10), 1114–1123. doi:10.1016/j.cemconcomp.2012.08.004

Sueki, S., Soranakom, C., Mobasher, B., and Peled, A. (2007). Pullout-slip Response of Fabrics Embedded in a Cement Paste Matrix. *J. Mater. Civ. Eng.* 19 (9), 718–727. doi:10.1061/(asce)0899-1561(2007)19:9(718)

Victor, C. L., and Forii, H. (1993). From Micromechanics to Structural Engineering the Design of Cementitious Composites for Civil Engineering Applications. *Doboku Gakkai Ronbunshu* 1993 (471), 1.

Yang, E. H., Wang, S., Yang, Y., and Li, V. C. (2008). "Fiber-bridging Constitutive Law of Engineered Cementitious Composites". (Japan: Japan Concrete Institute).

Zhigang, Z. (2020a). Effect of Sub-elevated Temperature on Mechanical Properties of ECC with Different Fly Ash Contents. *Construction Building Mater.* 262, 120096. doi:10.1016/j.conbuildmat.2020.120096

Zhigang, Z. (2020b). SPEco-Friendly High Strength, High Ductility Engineered Cementitious Composites (ECC) with Substitution of Fly Ash by rice Husk Ash. *Cement Concrete Res.* 137, 106200. doi:10.1016/j.cemconres.2020.106200

Zhigang, Z. (2021). Sustainable High Strength, High Ductility Engineered Cementitious Composites (ECC) with Substitution of Cement by rice Husk Ash. *J. Clean. Prod.* 317, 128379. doi:10.1016/j.jclepro.2021.128379